BID regulates AIF-mediated caspase-independent necroptosis by promoting BAX activation

Santos A. Susin, Lauriane Cabon, Patricia Galan-Malo, Aida Bouharrour, Laure Delavallee, Marie-Noelle Brunelle-Navas, Hans K Lorenzo, Atan Gross

BID regulates AIF-mediated caspase-independent necroptosis by promoting BAX activation

Lauriane Cabon[1, 2, 3], Patricia Galan-Malo[1, 2, 3#], Aïda Bouharrour[1, 2, 3#], Laure Delavallée[1, 2, 3], Marie-Noëlle Brunelle-Navas[1, 2, 3], Hans K. Lorenzo[4, 5, 6], Atan Gross[7], and Santos A. Susin[1, 2, 3*]

[1] INSERM U872, Mort cellulaire programmée et physiopathologie des cellules tumorales, Equipe 19, Centre de Recherche des Cordeliers, Paris, France

[2] Université Pierre et Marie Curie-Sorbonne Universités, UMRS 872, Paris, France

[3] Université Paris Descartes, UMRS 872, Paris, France

[4] Faculté de Medécine, Université Paris 11, Le Kremlin-Bicêtre, France

[5] CHU Bicêtre, Service de Néphrologie, Le Kremlin-Bicêtre, France

[6] INSERM U1014, Villejuif, France

[7] Department of Biological Regulation, Weizmann Institute of Science, Rehovot, Israel

Running Title: BID controls MNNG-induced necroptosis

# Equal contribution

*Corresponding author: Santos A. Susin. Centre de Recherche des Cordeliers. 15, rue de l'Ecole de Médecine, 75006, Paris, France. Tel: +33 144279070; Fax: +33 144279036; E-mail: santos.susin@crc.jussieu.fr

ABSTRACT

Alkylating DNA damage agents such as MNNG trigger necroptosis, a newly defined form of programmed cell death (PCD) managed by RIP kinases. This caspase-independent mode of cell death involves the sequential activation of PARP-1, calpains, BAX and AIF, which redistributes from mitochondria to the nucleus to promote chromatinolysis. We have previously demonstrated that the BAX-mediated mitochondrial release of AIF is a critical step in MNNG-mediated necroptosis. However, the mechanism regulating BAX activation in this PCD is poorly understood. Employing mouse embryonic knockout cells, we reveal that BID controls BAX activation in AIF-mediated necroptosis. Indeed, BID is a link between calpains and BAX in this mode of cell death. Therefore, even if PARP-1 and calpains are activated after MNNG treatment, BID genetic ablation abolishes both BAX activation and necroptosis. These PCD defects are reversed by reintroducing the BID-wt cDNA into the *BID*$^{-/-}$ cells. We also demonstrate that, after MNNG treatment, BID is directly processed into tBID by calpains. In this way, calpain non-cleavable BID proteins (BID-G70A or BID-Δ68-71) are unable to promote BAX activation and necroptosis. Once processed, tBID localizes in the mitochondria of MNNG-treated cells, where it can facilitate BAX activation and PCD. Altogether, our data reveal that, as in caspase-dependent apoptosis, BH3-only proteins are key regulators of caspase-independent necroptosis.

Key Words: AIF, BAX, BID, Calpains, Necroptosis

When and how a cell dies is one of the essential questions to understand the biology of the cell. A cell is considered dead when the integrity of its plasma membrane is compromised, when its fragments are engulfed by an adjacent or a professional cell or when its components, including the nucleus, are fragmented. It is more complicated to outline how a cell could die. Historically, two major types of cell death have been distinguished: apoptosis, a controlled or programmed cell death (PCD), and necrosis, an uncontrolled or accidental death.[1] Cell biologists have particularly focused their attention on apoptotic PCD, helping to characterize it at both genetic and biochemical levels.[2] Fascinatingly, the use of apoptotic inhibitors or cells that are deficient in key apoptotic molecules has revealed the existence of new PCD pathways. As a consequence, active forms of cell death started to be referred to as caspase-dependent or caspase-independent.[3] More recently, it has been accepted that necrosis is more than an unregulated type of death. Indeed, a cell can use different mechanisms/pathways with underlying apoptotic or necrotic features to accomplish its proper demise.[4]

The analysis of the tumor necrosis factor (TNF) signaling path has shed new light on the existence of PCD pathways with necrotic features. When TNF binds its receptor (TNFR), two ways can be engaged: (i) caspase-dependent apoptosis, mediated by activation of caspase-8, and (ii) something similar to necrosis, which is caspase-independent, and is mediated by receptor interacting protein (RIP) kinases RIP1 and RIP3. Pharmacological and genetic approaches have revealed a panoply of modulators of TNF-induced necroptosis, a term used to define this finely regulated form of cell death.[5] Strikingly, PCD by necroptosis (programmed necrosis) is also induced by high doses of the alkylating DNA damage agent *N*-methyl-*N'*-nitro-*N'*-nitrosoguanidine (MNNG).[6] This necroptotic process, which is also regulated by the kinase RIP1,[7] is executed by the harmonic activation of poly(ADP-ribose) polymerase-1 (PARP-1), Ca^{2+}-dependent calpain Cys-proteases, and the pro-apoptotic BCL-2 member BAX.[8] A key consequence of the activation of these three enzymes is the mitochondrial release of truncated AIF (tAIF), a major effector in caspase-independent PCD.[9-13] Cytosolic tAIF rapidly redistributes to the nuclear compartment where, assisted by γH2AX and cyclophilin A (CypA), it promotes chromatinolysis and cell viability loss.[14, 15]

Among the features of MNNG-induced necroptosis, the implication of BCL-2 family members appears as a milestone. The BCL-2 set of proteins is distributed in three subgroups according to their properties.[16] The first subfamily comprises BCL-XL, BCL-2, BCL-W and MCL-1. They contain three or four BCL-2 homology (BH) domains that are known to be necessary for their anti-apoptotic function. Through their interactions with other BCL-2

members, they negatively regulate the mitochondrial release of pro-apoptotic proteins.[16] The second subgroup corresponds to pro-apoptotic proteins, such as BAX and BAK, which are able to form pores or associate with pore-forming proteins in the outer mitochondrial membrane. This process induces mitochondrial permeabilization and the release of cell death-promoting proteins.[17] The third BCL-2 subfamily regroups the proteins that only have a short BH3 domain. These BH3-only proteins interact with both anti- and pro-apoptotic BCL-2 members to induce PCD.[16]

In MNNG-induced necroptosis, the key role of the two first subgroups of the BCL-2 family has been recently established: BCL-2 and BAX manage the mitochondrial release of tAIF.[8] However, a pivotal question remains: How is BAX activated here? With the help of a panel of murine embryonic fibroblast (MEF) knockout cells, the aim of the present work was to examine this issue. This approach revealed that, through its pro-apoptotic function, BID regulates BAX activation and PCD. Cleaved into tBID *via* a calpain cleavage at Gly70, this BH3-only protein is indeed the link between calpains and BAX in MNNG-mediated necroptosis.

RESULTS

MNNG-induced caspase-independent necroptosis: a highly regulated PCD process

Treatment of MEFs with MNNG induces necroptosis, a RIP1 kinase-dependent mode of PCD modulated by necrostatin-1 (Supplementary Figure 1).[5-7] This type of cell death, enabled here by the action of PARP-1, is a caspase-independent process with significant alterations detected as soon as 6 h of MNNG treatment (Figure 1a).[8, 14] As in staurosporine (STS)-induced caspase-dependent apoptosis (our positive control), MNNG-treated cells undergo Annexin V-detectable phosphatidylserine (PS) exposure. However, in contrast to STS-induced PCD, MNNG treatment provokes a double Annexin V/PI positive labeling (Figure 1a), which is indeed a hallmark of this type of PCD.[18] MNNG-induced death is also characterized by the sequential activation of calpains and BAX (Figures 1b and c).[8] Once in mitochondria, BAX provokes a mitochondrial damage that is accompanied by the release of tAIF, the truncated form of AIF, to the cytosol and nucleus (Figures 1d and e).[8, 14] In the nucleus, this apoptogenic protein generates TUNEL-detectable 3'-OH DNA breaks in DNA (Figure 1f). Altogether, these events represent the biochemical hallmarks of MNNG-mediated necroptosis.[8, 14]

BAX activation is critical in MNNG-induced necroptosis

The presence of tAIF in extramitochondrial compartments is vital in the PCD process triggered by MNNG. As demonstrated by BAX genetic ablation, tAIF release and necroptosis are specifically controlled by the mitochondrial action of activated BAX (Figure 2a and b).[8] But, how is BAX activated in necroptosis? We have previously described that BAX activation depends on calpain activity.[8] Thus, a first possibility is that calpains cleave inactive BAX at Asp33 (D33) to yield a p18 active protein.[19] By an immunoblotting approach, we thus tested whether the treatment of MEFs with MNNG generated the p18 active form of BAX. As depicted in Figure 2c, in contrast to STS, BAX does not become cleaved at D33 even 9 h after MNNG-treatment. This result indicates that, in MNNG-induced necroptosis, BAX is not directly processed by calpains.

BID, but not BIM or BAD, is necessary for MNNG-induced BAX activation

The negative results represented in Figure 2c led us to analyze other possibilities for calpain-mediated BAX activation. Two manuscripts have already described that calpains control JNK1 activation[20] and that AIF is released from mitochondria by JNK1-mediated activation. [7] Moreover, it has been demonstrated that JNK phosphorylation and activation of the BH3-only proteins BIM and BAD couple the stress-activated signaling pathway to the BAX-dependent

cell death machinery.[21, 22] Thus, a working hypothesis is that calpains activate JNK1 which, by means of BIM or BAD phosphorylation, yields active BAX. A third BH3-only protein, BID, could also be implicated in calpain-mediated BAX activation. Indeed, calpains cleave BID in a 15-kDa fragment similar to the pro-apoptotic caspase-cleaved tBID.[23] Once generated, tBID could provoke mitochondrial AIF release.[13, 24, 25] Thus, a second BH3-only working hypothesis is that calpains cleave BID into tBID. Truncated BID could then regulate BAX activation, which provokes mitochondrial tAIF release and necroptosis.

We assessed the potential role of the BH3-only proteins BIM, BAD, and BID in MNNG-induced PCD by means of gene knockout MEFs. When comparing with WT, we observed that in *BIM*$^{-/-}$ or *BAD*$^{-/-}$ cells, both MNNG-induced necroptosis and BAX activation remained unaffected. In contrast, MNNG-induced BAX activation and death were efficiently delayed in *BID*$^{-/-}$ MEFs (Figures 3a-c). In these cells, the percentage of PS exposure and loss of viability reached ~10 % 9 h after MNNG treatment. At the same time, MNNG induced death in about 60 % of WT cells. As expected from the absence of BAX activation in *BID*$^{-/-}$ MEFs (Figure 3c), the presence of tAIF in extramitochondrial compartments was negative (Figure 3d). As internal control, we confirmed that WT, *BIM*$^{-/-}$, *BAD*$^{-/-}$, and *BID*$^{-/-}$ cells treated with the caspase-dependent apoptosis inducer STS displayed similar cell death levels (Figure 3a), confirming that these MEFs remained sensitive to other PCD inducers. In any case, BID and not BIM or BAD deficiency disabled BAX activation and necroptosis.

By reintroducing BID-wt cDNA into *BID*$^{-/-}$ cells by lentiviral transduction, we corroborated that the loss of the BAX-dependent necroptotic hallmarks was due to the specific lack of BID. Indeed, BID-wt cDNA transduction fully resensitized *BID*$^{-/-}$ cells to MNNG-mediated PCD, including mitochondrial damage, BAX activation, TUNEL positivity, and cell viability loss (Figures 4a-d).

The BAX-dependent necroptotic hallmarks are abolished in MNNG-treated *BID*$^{-/-}$ MEFs

To gain insights into the role of BID in the MNNG-mediated PCD pathway, we next determined whether the absence of BID exclusively affected BAX activation or if, on the contrary, BID deficiency disabled other key necroptotic events. We first verified whether PARP-1 and calpains, which act upstream of BAX in MNNG-mediated PCD, were activated or not in *BID*$^{-/-}$ MEFs. PARP-1 activation is assessed by the inverse relationship existing between poly(ADP-ribose) (PAR) and NAD^+ and ATP cellular levels. Note that we have previously demonstrated that the specific activation of PARP-1 in MNNG-mediated necroptosis is responsible for both the synthesis of the PAR polymers observed and the

depletion of NAD^+ and ATP cellular pools.[8] As shown by the formation of PAR polymers, PARP-1 was equally activated in WT and *BID*$^{-/-}$ MEFs (Figures 5a and b). This demonstrated that, even in the absence of BID, PARP-1 is an active enzyme. In line with that, MNNG caused a rapid and similar decrease in NAD^+ and ATP cellular levels in both WT and *BID*$^{-/-}$ MEFs (Figures 5c and d). The specificity of the PARP-1-dependent NAD^+ loss associated with MNNG treatment in these cells was confirmed using a pharmacological PARP inhibitor, PJ34. Meanwhile, calpain activity was measured with the help of a cell-permeable substrate that reports calpain activity in live cells. This approach showed that MNNG induced rapid calpain activation in WT and *BID*$^{-/-}$ MEFs (Figure 5e). Overall, these results indicate that *BID*$^{-/-}$ MNNG-treated MEFs activate PARP-1 and calpains in exactly the same way as WT cells. In contrast, MNNG-treated *BID*$^{-/-}$ MEFs never present BAX-dependent necroptotic hallmarks: $\Delta\Psi$m drop, tAIF release, and TUNEL positivity (Figures 5f-h).

These data raised an additional question: how can MNNG-treated *BID*$^{-/-}$ MEFs be viable with activated PARP-1/calpains, consumed NAD^+/ATP pools, and massive DNA damage (assessed by a COMET assay, Supplementary Figure 2a)? To answer this question, we performed long-term experiments in MNNG-treated WT and *BID*$^{-/-}$ MEFs. As depicted in Supplementary Figure 2b, at 12 h post MNNG treatment 98% of WT MEFs were necroptotic. In contrast, only ~20% of *BID*$^{-/-}$ cells exposed the characteristic double Annexin/PI positive labeling. Strikingly, a significant population of *BID*$^{-/-}$ MEFs (~45/50%) remained viable even 24 h post MNNG incubation (Supplementary Figures 2b and c). The rest of the *BID*$^{-/-}$ population exploded (Supplementary Figure 2d). Overtime, similarly to what has been previously reported for MNNG-treated *H2AX*$^{-/-}$ MEFs,[14] it seems that the cell is unable to achieve the necroptotic PCD program in the absence of BID. As a result, the "highly damaged" cell, which is unable to proliferate/divide (Supplementary Figure 3), explodes by an uncontrolled form of necrosis.

Altogether, our results identify BID as a key component of MNNG-induced necroptosis. By controlling BAX activation, BID manages this type of PCD.

MNNG-induced DNA damage and necroptosis is not influenced by the pro-survival function of BID

BID is not only a pivotal executioner of PCD. In response to a DNA double-strand breaks (DSB) damage such as that triggered by etoposide, BID activates a pro-survival cell cycle regulatory activity mediated by its phosphorylation at Ser61 and 78 (S61 and S78).[26, 27] Thus, to achieve the characterization of the role of BID in MNNG-induced DNA-damage, which

also provokes DSB in DNA,[14] we evaluated the relevance of the pro-survival role of BID. Specific immunoblotting detection successfully revealed a time-dependent BID phosphorylation in MNNG-treated cells (Supplementary Figure 3a), suggesting that the pro-survival role of BID was enabled. We explored this possibility by a cell cycle analysis performed in MNNG-treated WT and *BID*$^{-/-}$ cells. Surprisingly, contrary to what had been previously reported for etoposide,[26] the percentages of the different cell cycle phases remained similar before and after MNNG treatment in both cell types (Supplementary Figures 3b, c and 4). This result opens two possibilities: (i) MNNG treatment causes the arrest of the cell cycle or (ii) this alkylating agent does not alter the cellular cycling at all. We verified these two alternatives by a BrdU/PI assessment. As revealed by the absence of proliferating cells, treatment with MNNG provoked the cell cycle halt in both WT and *BID*$^{-/-}$ MEFs (Supplementary Figure 3d). Altogether, our results differentiate the response of *BID*$^{-/-}$ cells to MNNG and etoposide, and suggest that necroptosis is not modulated by the cell cycle/DNA repair mechanisms implicating phosphorylated BID. This is substantiated by a flow cytometry assessment performed in *BID*$^{-/-}$ MEFs stably transfected with BID-wt or a non-phosphorylatable BID-S61A/S78A cDNA (Ser61 and 78 of BID-wt were mutated to Ala). Our data show that, contrary to what has been reported after etoposide DSB generation, MNNG does not induce a different rate of necroptosis in *BID*$^{-/-}$ cells expressing BID-S61A/S78A or *BID*$^{-/-}$ cells expressing BID-wt (Supplementary Figure 3e). Therefore, we conclude that the phosphorylation of BID does not regulate the response of MEFs to the DNA damage provoked by MNNG. This necroptosis is exclusively modulated by the apoptogenic function of BID.

BID is cleaved into tBID by calpains in MNNG-mediated necroptosis

As indicated above, the pro-apoptotic properties of the BH3-only protein BID are pivotal in the BAX activation that controls caspase-independent necroptosis. In apoptotic caspase-dependent PCD, this apoptogenic action is generally arbitrated by the caspase-cleaved BID, tBID.[28, 29] In apoptotic PCD, tBID plays a double role in BAX activation. On the one hand, tBID opens the N-terminal moiety of BAX.[30] On the other hand, tBID redistributes to mitochondria where it favors BAX recruitment and activation.[16, 31, 32] Hence, it seems mandatory to verify whether, in MNNG-treated MEFs, BID exerts its BAX activation function by means of the truncated form. As indicated in Figure 6a, a kinetic immunoblot analysis performed with a specific antibody demonstrated that a fraction of BID became cleaved into tBID after MNNG-treatment. The time-dependent tBID generation correlated to

MNNG-induced necroptosis (Figures 1a). Moreover, as was to be expected, tBID localized in mitochondria, where it was able to achieve its BAX-activating function (Figures 6a, right panels).

How does BID become activated/cleaved in caspase-independent necroptosis? Are calpains implicated in this cleavage? To answer these questions, we first tested whether BID was cleaved in calpain-inactivated knockout MEFs (*CAPN4*$^{-/-}$).[20] As depicted in Figure 6b, MNNG-induced BID cleavage was abolished in *CAPN4*$^{-/-}$ cells. Note that these cells treated with STS displayed similar levels of tBID to WT cells. This confirmed that BID could be caspase-dependent cleaved in *CAPN4*$^{-/-}$ MEFs. Interestingly, as could be expected from the absence of tBID in MNNG-treated *CAPN4*$^{-/-}$ MEFs, BAX activation, $\Delta\Psi_m$ drop, PS exposure, and cell viability loss were also negative (Figures 6c-e). These results place BID between calpains and BAX in this mode of death and indicate that calpains are implicated in the tBID generation associated to MNNG-mediated PCD.

Indeed, is BID directly cleaved into tBID by calpains or is tBID generated by a protease downstream of calpains? To fully analyze these two possibilities we assessed whether calpain non-cleavable (nc) BID restored MNNG-mediated necroptosis in BID$^{-/-}$ MEFs. The reactivation of MNNG-mediated necroptosis in these cells would indicate that a protease other than calpains generates the processed fragment of BID. The opposite result (calpain ncBID is not processed into tBID after MNNG treatment and is unable to restore PCD) would indicate that BID is directly cleaved into tBID by calpains to promote BAX activation. To design the calpain ncBID vectors, we took into consideration theoretical sequential/structural determinants of calpain-mediated cleavage[33] and previous work suggesting that calpains processed BID into tBID at position Gly70.[34] Thus, we generated two constructs: BID-G70A, which contains the Gly70 mutated to Ala, and BID-Δ68-71, in which the entire "calpain cleavable region of BID" has been deleted. Note that, similarly to the caspase-mediated BID cleavage occurring at D59 position,[28] the cleavage at G70 provoked the removal of the BID N-terminus and exposed the amphipathic α helix BH3 on the active C-terminal tBID p15 fragment (Figure 7a). As illustrated in Figures 7b-e and Supplementary Figure 5, transduction of *BID*$^{-/-}$ MEFs with lentiviruses carrying vectors of BID-wt, a caspase ncBID-D59A mutant,[35] or the two calpain ncBID mutants defined above revealed that: (i) BID-wt and BID-D59A re-sensitized *BID*$^{-/-}$ cells to MNNG-induced necroptosis. This confirmed our results showing that AIF-mediated necroptosis is a caspase-independent mode of PCD promoted by BID; (ii) BID-G70A and BID-Δ68-71 transduction does not restore the

MNNG ability to induce necroptosis in $BID^{-/-}$ MEFs; and (iii) as was to be expected, BID-wt and BID-D59A are processed after MNNG treatment. On the contrary, BID-G70A and BID-Δ68-71 remain as precursor proteins. Note that *$BID^{-/-}$* cells transduced with calpain ncBID mutants retain the apoptotic function (Supplementary Figure 6). Altogether, these data reveal that, in AIF-mediated necroptosis, calpains cleave BID into tBID at Gly70. The mutation/deletion of the calpain cleavage site of BID is sufficient to prevent BID processing, BAX activation, mitochondrial damage, and cell viability loss.

DISCUSSION

The present work uncovers a milestone in understanding the molecular mechanisms that regulate the necroptotic pathway induced by MNNG: the pivotal role of the BH3-only protein BID. Together with our previous results[8, 14], our present data provide a detailed sequence of events for DNA damage-mediated necroptosis: MNNG treatment induces a PARP-1 hyperactivity that leads to calpain activation. Calpains generate the cleaved form of BID (tBID), which redistributes from the cytosol to mitochondria, where it regulates BAX activation. Once activated, BAX provokes mitochondrial damage and tAIF mitochondrial release. tAIF relocalizes to the nucleus and, associated to γH2AX and CypA, induces chromatinolysis and cell viability loss (Figure 8).

This work strengthens the idea that necroptosis is underpinned by a paradoxal PCD program, which is different from but similar to the broadly studied apoptotic program. It is different from apoptosis in as much as necroptosis substitutes caspases for calpains, enables a specific DNA-degrading module, and generates a controlled double AnnexinV/PI labeling.[18] It is similar to apoptosis because mitochondria plays a pivotal role and operates under the control of typical apoptotic molecules (e.g. PARP-1, BID, BCL-2, BAX). The apoptotic and the necroptotic pathways therefore represent alternate outcomes of similar PCD programs.

When assessing how BAX could be activated in necroptosis induced by high doses of MNNG, we have focused on calpains.[8] Ruling out the hypothesis of the direct activation of BAX by calpain cleavage, and keeping in mind that BCL-2 and BAX regulate MNNG-mediated PCD, we have examined the third subfamily of BCL-2 proteins: the BH3-only subgroup. More precisely, our attention was directed to BAD, BIM and BID, three BH3-only proteins that could be activated by calpains. In this sense, our data willingly demonstrate that BAD and BIM are dispensable, whereas BID is essential to MNNG-induced necroptosis. More precisely, our data reveal that the Ca^{2+}-dependent calpain Cys proteases control BAX activation via a cleavage of BID into tBID at Gly70. Notably, a single mutation in this amino acid is sufficient to preclude AIF-mediated necroptosis. This is an important finding that provides a major target in this PCD program. Additionally, calpain inhibitors and calcium chelators are now evinced as attractive tools in the regulation of the necroptotic pathway.

BID appears to link PARP-1 and calpains activity to BAX activation and tAIF-release in MNNG-mediated necroptosis. This is a key issue because the presence of tAIF in the cytosol and further in the nucleus is essential to the generation of the DNA-degrading complex that manages necroptosis.[14] These findings are in line with previous work on the

relationships between BID and tAIF performed on purified mitochondria, on neuronal cell death induced by excitotoxic stimuli, oxidative stress, β-amyloid exposure, and on breast cancer cell death exposed to photodynamic therapy.[13, 24, 25, 36, 37]

As part of the molecular exploration of necroptosis, this work is indeed a first step in the analysis of the role of the BH3-only protein BID. Ensuing questions arise: could BID favor AIF mitochondrial release by altering the mitochondrial morphology, as in other apoptotic systems?[25] Are MTCH2/MIMP[38] implicated in the mitochondrial recruitment of tBID in necroptosis? Future steps in the study of this BH3-only protein in necroptosis will unravel the mechanisms that control BID-mediated BAX activation and AIF-release, and will evaluate whether these mechanisms are similar in caspase-dependent and caspase-independent PCD.

Together with BID, two other BH3-only proteins have already been related to cell death programs with necrotic morphology: BMF and BNIP3.[39, 40] Their existence brings new perspectives to the development of small molecules mimicking the activity of BH3-only proteins. Compounds such as Gossypol, ABT-263 or GX15-070 have been designed to overcome the overexpression of anti-apoptotic proteins in cancer cells. If these BH3-mimetics can also target necroptotic pathways, such drugs could find wider applications than initially expected. In this sense, the implication of necroptosis is described in brain ischemia, myocardial infarction, neurodegenerative diseases, head trauma, therapeutic killing of tumor cells, etc.[5, 6] Thus, by shedding new light on the mechanisms regulating necroptosis, our new findings pave the way for novel pharmacological strategies that could target aberrant PCD. Furthermore, our work introduces the concept that, as in classical apoptosis, the entire BCL-2 family of proteins is at the crossroads of the necroptotic pathways.

MATERIALS AND METHODS

Cell culture and cell death induction and inhibition

Murine embryonic fibroblasts (MEFs) were cultured in DMEM supplemented with 10% FCS, 2 mM L-glutamine, and 100 U/ml penicillin/streptomycin (Invitrogen), and maintained at 37°C in a 5% CO_2 atmosphere. *BAX*$^{-/-}$ MEFs were provided by SJ Korsmeyer (Dana-Farber Cancer Institute, USA), *BIM*$^{-/-}$ by DC Huang (Walter and Eliza Hall Institute, Australia), *BAD*$^{-/-}$ by NN Danial (Harvard Medical School, USA), *CAPN4*$^{-/-}$ by PA Greer (Queen's University, Canada), and *RIP1*$^{-/-}$ by MA Kelliher (UMass Medical School, USA). *BID*$^{-/-}$, *BID*$^{-/-}$ MEFs stably transfected with BID-wt or a non-phosphorylatable BID-S61A/S78A were previously described.[26] *BAX*$^{-/-}$, *BIM*$^{-/-}$, *BAD*$^{-/-}$, *BID*$^{-/-}$, and *RIP1*$^{-/-}$ MEFs are derived from C57BL/6 mice and *CAPN4*$^{-/-}$ from 129SvJ mice. *BAX*$^{-/-}$, *BIM*$^{-/-}$, *BAD*$^{-/-}$, and *BID*$^{-/-}$ are SV40 immortalized. *RIP1*$^{-/-}$ and *CAPN4*$^{-/-}$ MEFs were immortalized by a classical 3T3 dilution method. WT cells from each lineage were used as a control.

To induce death, cells were treated with MNNG (500 μM, ABCR GmbH) for 20 min. The treating medium was replaced after incubation by a fresh medium devoid of MNNG, and cells (80% confluence) were cultured at the indicated times. As a control of caspase-dependent apoptosis, cells were incubated 6 h with STS (1 μM) or etoposide (20 μM) or 9 h with TNF/CHX (50 ng.ml/1μg.ml). In some experiments, cells were pre-incubated 1 h with Q-VD.OPh (QVD, 10 μM, MP Biomedicals) or necrostatin-1 (10 μM) before treatment.

Vectors and lentiviral transduction

Murine BID-wt, BID-D59A, BID-G70A, and BID-Δ68-71 cDNAs tagged with a V5 epitope were cloned into the pLVX-IRES-Zs-Green lentiviral vector (Clontech). Viruses were produced into 293T cells by $CaCl_2$ transient transfection of the lentiviral constructs and the packaging plasmids pMD2.G and psPAX-2 (Addgene plasmids 12259 and 12260, respectively). 48 h after transfection, lentiviral supernatants were harvested, clarified by filtration, and used immediately for *BID*$^{-/-}$ MEFs transduction with 4 μg/mL of polybrene. 72 h after transduction, cells were diluted for immunoblot selection of individual clones. Clones with similar BID levels to WT BID MEFs were selected, expanded, and analyzed.

Flow cytometry

We used Annexin V-APC (0.1 μg/ml) for the assessment of PS exposure, propidium iodide (PI, 0.5 μg/ml) for cell viability analysis, and tetramethylrhodamine ethyl ester (TMRE, 20 nM) for $\Delta\Psi$m quantification. Cell death was recorded in a FACSCanto II (BD Biosciences) in the total population (10,000 cells) and data were analyzed using FlowJo software.

Determination of ATP content

Cells treated as indicated above were lysed and the total ATP content was assessed with a luciferin-luciferase kit. Luminiscence was measured in a Berthold LB96V MicroLumat Plus. ATP content is

expressed as relative to the number of cells analyzed in arbitrary units. 100% refers to the ATP quantified in control cells.

Poly(ADP ribose) assessment

For immunoblotting detection, $1x10^6$ cells were lysed in RIPA buffer containing 25 mM Tris-HCl (pH 6.0), 150 mM NaCl, 1% Sodium Deoxycholate, 0.1% SDS, and 1% NP-40. Samples were resolved on 5-8% SDS polyacrylamide gels and transferred onto a PVDF membrane using a semi-dry method. Membrane blocking and antibody incubations were performed in PBS 0.1% Tween 20 plus 5% non-fat dry milk. Membranes were probed with an anti-PAR antibody (Clone 10H, Alexis), immunoreactive proteins were detected by an HRP-conjugated anti-mouse antibody, and revealed by enhanced chemiluminescence (ECL, Pierce).

Alternatively, cells seeded on coverslips were fixed in ice-cold methanol for 15 min, permeabilized with 0.1% Triton X-100, pre-incubated in 10% goat serum for 30 min, incubated with the anti-PAR antibody, and detected by anti-rabbit IgG conjugated with Alexa® Fluor 488 (Invitrogen). Before assessment, cells were co-stained with Hoechst 33342 and mounted with FluorSave (Calbiochem). Green and blue fluorescences were recorded in a confocal microscope (LSM-510 Meta, Zeiss). Quantification was performed on 150 cells for each data point.

Calpain activity

Calpain activity present in 30 μg of total cell lysates was determined by cleavage of the fluorescent substrate N-succinyl-LLVY-AMC (Calbiochem) and expressed as the difference between calcium-dependent and calcium-independent fluorescence. Calcium-dependent fluorescence was measured after 30 min incubation at 37 °C in buffer containing 63 mM imidazole-HCl (pH 7.3), 10 mM β-mercaptoethanol and 5 mM $CaCl_2$. Calcium-independent fluorescence was measured under the same conditions using buffer without $CaCl_2$ and containing 1 mM EDTA and 10 mM EGTA. Fluorescence was recorded in a Fluoroskan Ascent™ Fluorimeter.

Calpain activity in live cells was detected using the cell-permeable calpain substrate Boc-Leu-Met-CMAC (Invitrogen). Cells spread on coverslides were incubated for 30 min with 50 μM of calpain substrate in DMEM culture medium. Cells were then treated or not with MNNG and observed in a Nikon Eclipse TE2000-U microscope. Quantification was performed on 100 cells for each data point.

BAX activation and redistribution

For flow cytometry or immunofluorescence analysis, cells were fixed in 1% paraformaldehyde (PFA), permeabilized with 0.1 % saponin for 10 min, incubated 1 h with an antibody designed against the active form of BAX (clone 6A7, BD Biosciences, ref# 556467), and detected by an anti-mouse IgG conjugated with Alexa® Fluor 488 or 647. Cells were either analyzed by cytofluorometry or stained with Hoechst 33342 and incubated with Mitotracker Red previous to fixation for immunofluorescence assessment. Images were acquired with a confocal microscope as above. Quantification was performed on 100 cells for each data point.

3'-OH DNA breaks (TUNEL) detection

Detection of blunt double-stranded fragments carrying a 5′-phosphate and 3′-hydroxyl group was carried out by fixing cells in freshly prepared 1% PFA for 30 min at 4 °C and permeabilized with 0.1% Triton X-100 and 0.1% sodium citrate for 10 min at 4 °C. After washing in PBS containing 1% BSA, cells were incubated for 1 h at 37°C with 50 µl of a reaction mixture containing 0.025 nmol of Fluorescein-12-dUTP (Roche) or CF™ 640R-dUTP (Biotium), 0.25 nmol of dATP, 2.5 mm $CoCl_2$, 80 units of recombinant terminal deoxynucleotidyl transferase (TdT) and TdT reaction buffer from Roche. After being washed in PBS, cells were analyzed by flow cytometry.

BID modeling

BID structure (pdb 1DDB) was modeled in SwissPDBViewer and the resulting model was edited with Pymol, as previously described.[14]

Single cell gel electrophoresis (COMET)

Neutral comet assay was performed with a kit from Trevigen following the manufacturer's instructions. Single cell images were captured and analyzed using a Nikon Eclipse TE2000-U microscope as indicated above. Quantification was performed on 100 cells for each data point.

MTT cell viability

3-(4,5-Dimethylthiazol-2-yl)-2,5-diphenyltetrazolium bromide (MTT, 0.5 mg/ml final concentration) was added to the culture medium of cells growing in 96-well dishes (6,000 cells/well). After incubating the dishes at 37°C for 90 min, the assay was stopped by adding 100 μl DMSO. Formazan salts were allowed to dissolve in DMSO shaking them gently for 10 min at room temperature, and the assays were quantified by means of a Multiskan plate reader (ThermoLabsystems, Cergy Pontoise, France). Final values were the result of subtracting 630 nm from 590 nm readings.

Cell cycle analysis and BrdU staining

Cells were harvested, washed once in PBS, fixed in ice-cold ethanol, and kept at -20°C. DNA contents were assessed by using PI (20 μg/mL) after 20 min incubation with RNAse A (160 μg/mL).

To determine DNA synthesis, cells were pulse-labeled with 30 μM BrdU for 30 min. Cells were fixed for at least 16 h and membranes were digested with 0.05% pepsin in 30 mM HCl at 37°C for 20 min. To allow the access of anti-BrdU antibody to the incorporated BrdU, DNA denaturation by 2N HCl was performed for 20 min at room temperature (RT). Following centrifugation, acid was neutralized by adding 0.1 M sodium borate for 4 min. Cells were then centrifuged, washed, and FITC-conjugated anti-BrdU antibody (BD Biociences) was added for 45 min at RT. The incubation buffer used was 20 mM HEPES, 0.5% FCS, 0.5% Tween 20. DNA was stained with PI before flow cytometer analysis.

Protein extraction, cell fractionation, immunoblotting, and quantification of mitochondrial tBID

For whole protein extracts, $1x10^6$ cells were lysed in buffer containing 20 mM Tris-HCl (pH 7.6), 150 mM NaCl, and 1% Triton X-100. For cytosolic purification, $2x10^6$ cells were resuspended in buffer

containing 220 mM mannitol, 70 mM sucrose, 50 mM Hepes-KOH (pH 7.2), 10 mM KCl, 5 mM EGTA, 2 mM MgCl2, and 0.025% digitonin, and kept on ice for 5 min. Lysed cells were centrifuged (16,000 *g*, 5 min, 4 °C) and the supernatant was retained as cytosolic fraction. Mitochondrial fractions were obtained using the Mitochondria Isolation kit from Pierce following the manufacturer's instructions. Protein concentration was determined using the BioRad Protein Assay. Equal amounts of total proteins (40 to 100 μg) were loaded on 4-12% NuPAGE or linear SDS-PAGE gels and transferred onto a PVDF membrane. Membrane blocking and antibody incubations were performed in PBS 0.1% Tween 20 plus 5% non-fat dry milk. The primary antibodies used were: BAX (specific for BAX p18 detection, BD Biosciences), AIF, BID/tBID (clone 14F2 Novus or AF860 R&D Systems), phospho BIDS78, phospho BIDS61 (Bethyl), pan-ERK (BD Biosciences), Cox IV subunit VIb (Invitrogen), V5 (clone V5-10), or β-actin (clone AC-15). Immunoreactive proteins were detected using HRP-conjugated secondary antibodies and revealed by the ECL system. In some experiments, equal loading was confirmed by staining the membrane with naphtol blue. Immunoblot images were adquired in a Bio-Imaging System MF-ChemiBis 4.2 or in a Kodax X-OMAT 1000 processor.

Statistics

Statistical analysis was carried out using the student's *t*-test.

Chemicals and reagents were purchased from Sigma-Aldrich except where otherwise noted.

ACKNOWLEDGEMENTS

We are grateful to Drs. SJ Korsmeyer, NN Danial, DCS Huang, PA Greer, and MA Kelliher for immortalized MEFs, RS Moubarak for preliminary data, and M Segade for proofreading. This work was supported by Agence Nationale de la Recherche (ANR; contract ANR-09-BLAN-0247), Association pour la Recherche sur le Cancer (ARC; contracts 5104 and 7987), Ligue Contre le Cancer, and Fondation de France (to SA Susin). L Cabon receives a PhD fellowship from École Normale Supérieure de Cachan (ENS-Cachan).

CONFLICT OF INTEREST

The authors declare no conflict of interest.

REFERENCES

1. Kerr JF, Wyllie AH, Currie AR. Apoptosis: a basic biological phenomenon with wide-ranging implications in tissue kinetics. *Br J Cancer* 1972; **26**(4)**:** 239-57.
2. Hengartner MO. The biochemistry of apoptosis. *Nature* 2000; **407**(6805)**:** 770-6.
3. Jaattela M. Programmed cell death: many ways for cells to die decently. *Ann Med* 2002; **34**(6)**:** 480-8.
4. Festjens N, Vanden Berghe T, Vandenabeele P. Necrosis, a well-orchestrated form of cell demise: signalling cascades, important mediators and concomitant immune response. *Biochim Biophys Acta* 2006; **1757**(9-10)**:** 1371-87.
5. Vandenabeele P, Galluzzi L, Vanden Berghe T, Kroemer G. Molecular mechanisms of necroptosis: an ordered cellular explosion. *Nat Rev Mol Cell Biol* 2010; **11**(10)**:** 700-14.
6. Delavallee L, Cabon L, Galan-Malo P, Lorenzo HK, Susin SA. AIF-mediated caspase-independent necroptosis: A new chance for targeted therapeutics. *IUBMB Life* 2011; **63**(4)**:** 221-32.
7. Xu Y, Huang S, Liu ZG, Han J. Poly(ADP-ribose) Polymerase-1 Signaling to Mitochondria in Necrotic Cell Death Requires RIP1/TRAF2-mediated JNK1 Activation. *J Biol Chem* 2006; **281**(13)**:** 8788-95.
8. Moubarak RS, Yuste VJ, Artus C, Bouharrour A, Greer PA, Menissier-de Murcia J *et al*. Sequential Activation of Poly(ADP-Ribose) Polymerase 1, Calpains, and Bax Is Essential in Apoptosis-Inducing Factor-Mediated Programmed Necrosis. *Mol Cell Biol* 2007; **27**(13)**:** 4844-62.
9. Susin SA, Lorenzo HK, Zamzami N, Marzo I, Snow BE, Brothers GM *et al*. Molecular characterization of mitochondrial apoptosis-inducing factor. *Nature* 1999; **397**(6718)**:** 441-6.
10. Norberg E, Orrenius S, Zhivotovsky B. Mitochondrial regulation of cell death: processing of apoptosis-inducing factor (AIF). *Biochem Biophys Res Commun* 2010; **396**(1)**:** 95-100.
11. Cregan SP, Fortin A, MacLaurin JG, Callaghan SM, Cecconi F, Yu SW *et al*. Apoptosis-inducing factor is involved in the regulation of caspase-independent neuronal cell death. *J Cell Biol* 2002; **158**(3)**:** 507-17.
12. Zhu C, Wang X, Huang Z, Qiu L, Xu F, Vahsen N *et al*. Apoptosis-inducing factor is a major contributor to neuronal loss induced by neonatal cerebral hypoxia-ischemia. *Cell Death Differ* 2007; **14**(4)**:** 775-84.
13. Culmsee C, Zhu C, Landshamer S, Becattini B, Wagner E, Pellecchia M *et al*. Apoptosis-inducing factor triggered by poly(ADP-ribose) polymerase and Bid mediates neuronal cell death after oxygen-glucose deprivation and focal cerebral ischemia. *J Neurosci* 2005; **25**(44)**:** 10262-72.
14. Artus C, Boujrad H, Bouharrour A, Brunelle MN, Hoos S, Yuste VJ *et al*. AIF promotes chromatinolysis and caspase-independent programmed necrosis by interacting with histone H2AX. *EMBO J* 2010; **29**(9)**:** 1585-99.

15. Baritaud M, Boujrad H, Lorenzo HK, Krantic S, Susin SA. Histone H2AX: The missing link in AIF-mediated caspase-independent programmed necrosis. *Cell Cycle* 2010; **9**(16)**:** 3166-73.

16. Chipuk JE, Moldoveanu T, Llambi F, Parsons MJ, Green DR. The BCL-2 family reunion. *Mol Cell* 2010; **37**(3)**:** 299-310.

17. Martinou JC, Green DR. Breaking the mitochondrial barrier. *Nat Rev Mol Cell Biol* 2001; **2**(1)**:** 63-7.

18. Boujrad H, Gubkina O, Robert N, Krantic S, Susin SA. AIF-mediated programmed necrosis: a highly regulated way to die. *Cell Cycle* 2007; **6**(21)**:** 2612-9.

19. Gao G, Dou QP. N-terminal cleavage of bax by calpain generates a potent proapoptotic 18-kDa fragment that promotes bcl-2-independent cytochrome C release and apoptotic cell death. *J Cell Biochem* 2000; **80**(1)**:** 53-72.

20. Tan Y, Dourdin N, Wu C, De Veyra T, Elce JS, Greer PA. Ubiquitous calpains promote caspase-12 and JNK activation during endoplasmic reticulum stress-induced apoptosis. *J Biol Chem* 2006; **281**(23)**:** 16016-24.

21. Donovan N, Becker EB, Konishi Y, Bonni A. JNK phosphorylation and activation of BAD couples the stress-activated signaling pathway to the cell death machinery. *J Biol Chem* 2002; **277**(43)**:** 40944-9.

22. Putcha GV, Le S, Frank S, Besirli CG, Clark K, Chu B *et al*. JNK-mediated BIM phosphorylation potentiates BAX-dependent apoptosis. *Neuron* 2003; **38**(6)**:** 899-914.

23. Chen M, He H, Zhan S, Krajewski S, Reed JC, Gottlieb RA. Bid is cleaved by calpain to an active fragment in vitro and during myocardial ischemia/reperfusion. *J Biol Chem* 2001; **276**(33)**:** 30724-8.

24. Landshamer S, Hoehn M, Barth N, Duvezin-Caubet S, Schwake G, Tobaben S *et al*. Bid-induced release of AIF from mitochondria causes immediate neuronal cell death. *Cell Death Differ* 2008; **15**(10)**:** 1553-63.

25. Tobaben S, Grohm J, Seiler A, Conrad M, Plesnila N, Culmsee C. Bid-mediated mitochondrial damage is a key mechanism in glutamate-induced oxidative stress and AIF-dependent cell death in immortalized HT-22 hippocampal neurons. *Cell Death Differ* 2010; **18**(2)**:** 282-92.

26. Kamer I, Sarig R, Zaltsman Y, Niv H, Oberkovitz G, Regev L *et al*. Proapoptotic BID is an ATM effector in the DNA-damage response. *Cell* 2005; **122**(4)**:** 593-603.

27. Zinkel SS, Hurov KE, Ong C, Abtahi FM, Gross A, Korsmeyer SJ. A role for proapoptotic BID in the DNA-damage response. *Cell* 2005; **122**(4)**:** 579-91.

28. Gross A, Yin XM, Wang K, Wei MC, Jockel J, Milliman C *et al*. Caspase cleaved BID targets mitochondria and is required for cytochrome c release, while BCL-XL prevents this release but not tumor necrosis factor-R1/Fas death. *J Biol Chem* 1999; **274**(2)**:** 1156-63.

29. Li H, Zhu H, Xu CJ, Yuan J. Cleavage of BID by caspase 8 mediates the mitochondrial damage in the Fas pathway of apoptosis. *Cell* 1998; **94**(4)**:** 491-501.

30. Cartron PF, Gallenne T, Bougras G, Gautier F, Manero F, Vusio P *et al*. The first alpha helix of Bax plays a necessary role in its ligand-induced activation by the BH3-only proteins Bid and PUMA. *Mol Cell* 2004; **16**(5)**:** 807-18.

31. Giam M, Huang DC, Bouillet P. BH3-only proteins and their roles in programmed cell death. *Oncogene* 2008; **27 Suppl 1:** S128-36.

32. Walensky LD, Pitter K, Morash J, Oh KJ, Barbuto S, Fisher J *et al*. A stapled BID BH3 helix directly binds and activates BAX. *Mol Cell* 2006; **24**(2)**:** 199-210.

33. Tompa P, Buzder-Lantos P, Tantos A, Farkas A, Szilagyi A, Banoczi Z *et al*. On the sequential determinants of calpain cleavage. *J Biol Chem* 2004; **279**(20)**:** 20775-85.

34. Mandic A, Viktorsson K, Strandberg L, Heiden T, Hansson J, Linder S *et al*. Calpain-mediated Bid cleavage and calpain-independent Bak modulation: two separate pathways in cisplatin-induced apoptosis. *Mol Cell Biol* 2002; **22**(9)**:** 3003-13.

35. Sarig R, Zaltsman Y, Marcellus RC, Flavell R, Mak TW, Gross A. BID-D59A is a potent inducer of apoptosis in primary embryonic fibroblasts. *J Biol Chem* 2003; **278**(12)**:** 10707-15.

36. Polster BM, Basanez G, Etxebarria A, Hardwick JM, Nicholls DG. Calpain I induces cleavage and release of apoptosis-inducing factor from isolated mitochondria. *J Biol Chem* 2005; **280**(8)**:** 6447-54.

37. Vittar NB, Awruch J, Azizuddin K, Rivarola V. Caspase-independent apoptosis, in human MCF-7c3 breast cancer cells, following photodynamic therapy, with a novel water-soluble phthalocyanine. *Int J Biochem Cell Biol* 2010; **42**(7)**:** 1123-31.

38. Zaltsman Y, Shachnai L, Yivgi-Ohana N, Schwarz M, Maryanovich M, Houtkooper RH *et al*. MTCH2/MIMP is a major facilitator of tBID recruitment to mitochondria. *Nat Cell Biol* 2010; **12**(6)**:** 553-62.

39. Hitomi J, Christofferson DE, Ng A, Yao J, Degterev A, Xavier RJ *et al*. Identification of a molecular signaling network that regulates a cellular necrotic cell death pathway. *Cell* 2008; **135**(7)**:** 1311-23.

40. Burton TR, Gibson SB. The role of Bcl-2 family member BNIP3 in cell death and disease: NIPping at the heels of cell death. *Cell Death Differ* 2009; **16**(4)**:** 515-23.

FIGURE LEGENDS

Figure 1 MNNG-induced caspase-independent necroptosis. (**a**) After the indicated time post MNNG or STS treatment, WT MEFs were stained with AnnexinV and PI, and the frequency of AnnexinV and PI positive labeling (% Cell death) was recorded by flow cytometry and illustrated as a plot. Data are the means of six independent experiments ± SD. Representative cytofluorometric plots are shown. Percentages in MNNG-treated cells refer to double positive staining and in STS-treated cells to AnnexinV and PI positive labeling. When indicated, WT MEFs were pre-incubated (1 h) with the pan-caspase inhibitor QVD before induction of cell death. Note that QVD inhibits STS-induced caspase-dependent apoptosis but not MNNG-mediated caspase-independent necroptosis. (**b**) Fluorometric analysis of calpain activity observed in cytosolic extracts obtained from WT treated with MNNG for the indicated times. One unit refers to basal calpain activity observed in untreated WT cells. Data are the mean of five independent experiments ± SEM. (**c**) Immunofluorescent staining of activated BAX detected in WT MEFs untreated (Control) or treated with MNNG (6 h). To visualize mitochondria, cells were incubated with Mitotracker Red prior to fixation. Hoechst 33342 was used to stain DNA. A representative overlay of activated BAX, MitoRed and Hoechst 33342 nuclear staining is shown. The number of cells presenting activated BAX were quantified and plotted as a percentage of total cells. Data are the means ± SD (n=5). Bar: 10 μm. Alternatively, MEFs were treated with MNNG for the indicated times, and BAX activation was measured by flow cytometry and illustrated as a bar chart. Data are the means ± SD (n=5). (**d**) Cells were treated with MNNG for the indicated times, then labeled with TMRE and assessed for $\Delta\Psi$m by flow cytometry. Results are the means of six independent experiments ± SD. In cytometry panels, percentages refer to cells with $\Delta\Psi$m loss. (**e**) Cytosolic fractions, recovered after MNNG-treatment, were blotted for tAIF detection. MNNG-treatment induces time-dependent tAIF release to cytosol. Actin (cytosolic marker) and Cox IV (mitochondrial marker) were used to control protein loading and fractionation quality. (**f**) At the indicated times after MNNG treatment, WT MEFs were stained for the detection of 3'-OH DNA breaks and analyzed by flow cytometry. Data are the means of five independent experiments ± SD. In representative cytofluorometric plots, percentages refer to TUNEL-positive cells.

Figure 2 The activation of BAX is a key step in necroptosis. (**a**) WT and *BAX*$^{-/-}$ MEFs were untreated (Control) or treated with MNNG (9 h) or STS, labeled with AnnexinV and PI,

and analyzed by flow cytometry. Representative plots are shown. Percentages in MNNG-treated cells refer to double positive staining and in STS-treated cells to AnnexinV and PI positive labeling. The red square highlights the absence of cell viability loss recorded in *BAX*$^{-/-}$ MEFs after MNNG treatment (**b**) Cells were stained as in **a**, and the frequency of AnnexinV and PI positive labeling (% Cell death) was recorded and expressed as a plot. Data are the mean of five independent experiments ± SD. *, $p<0.05$. (**c**) BAX immunoblotting detection in total extracts from WT MEFs untreated or treated with MNNG at different times. STS-treated cells were used as a positive control. The membrane was stained with naphtol blue (NB) to assess protein loading.

Figure 3 BID but not BIM or BAD deficiency disabled BAX activation and MNNG-induced necroptosis. (**a**) WT, *BIM*$^{-/-}$, *BAD*$^{-/-}$ and *BID*$^{-/-}$ MEFs were untreated (Control) or treated with MNNG (9 h) or STS, labeled with AnnexinV and PI, and analyzed by flow cytometry. Representative cytofluorometric plots are shown. The percentages refer to the frequencies of Annexin V and PI positive staining. (**b**) WT, *BIM*$^{-/-}$, *BAD*$^{-/-}$ and *BID*$^{-/-}$ MEFs were untreated (Control) or treated with MNNG (9 h), stained as in **a**, and the frequency of double positive labeling was recorded and expressed as a percentage. Data are the mean ± SEM (n=5). *, $p<0.05$. (**c**) WT, *BIM*$^{-/-}$, *BAD*$^{-/-}$ and *BID*$^{-/-}$ MEFs were treated with MNNG, and BAX activation was recorded by flow cytometry with the help of an α-Bax antibody (clone 6A7) specifically designed against the active conformation of BAX. Data in bar chart are the means of six independent experiments ± SD. *, $p<0.05$. Representative cytofluorometric plots of untreated (Control) and MNNG-treated (9 h) cells are shown. Percentages correspond to cells with active BAX. Note that, in the absence of α-Bax antibody, the labeling with the secondary antibody (Neg in cytofluorometric plots) yields negative results. The red squares in **a** and **c** highlight the absence of cell viability loss and BAX activation recorded in *BID*$^{-/-}$ MEFs after MNNG treatment. (**d**) Cytosolic fractions recovered from WT, *BIM*$^{-/-}$, *BAD*$^{-/-}$ and *BID*$^{-/-}$ MEFs untreated (Co) or treated with MNNG (9 h) were probed for tAIF detection. Actin was used to control protein loading.

Figure 4 Lentiviral transduction of *BID*$^{-/-}$ MEFs with V5 tagged BID-wt cDNA restores BAX activation and MNNG-induced necroptosis. (**a**) WT, *BID*$^{-/-}$, and two selected clones of *BID*$^{-/-}$ MEFs cells expressing BID-wt were untreated (Control) or treated with MNNG (9 h) and labeled with AnnexinV and PI. The frequency of double positive labeling was recorded and expressed as a plot. Data are the mean ± SD (n=4). *, $p<0.05$. The expression level of

BID in these cells was assessed by immunoblotting. Note the different apparent molecular mass of endogenous BID (~22 kDa) and lentiviral transduced BID-V5 (~26 KDa). Actin was used to control protein loading. (**b**) MEFs treated as in **a** were labeled with TMRE and assessed for $\Delta\Psi m$ by flow cytometry. The frequency of cells with $\Delta\Psi m$ loss was recorded and expressed as a plot. Data are the mean of four independent experiments ± SD. *, $p<0.05$. (**c**) The panel of MEFs used in **a** was untreated (Control) or MNNG-treated (9 h), and BAX activation was measured by flow cytometry and illustrated as a bar chart. Data are the means of four independent experiments ± SD. In representative cytofluorometric plots, percentages correspond to cells with active BAX. (**d**) MEFs were untreated (Control) or MNNG-treated (9 h), and the presence of 3'-OH DNA breaks was assessed by flow cytometry and illustrated as a plot. Data are the means of four independent experiments ± SD. In cytofluorometric plots, percentages correspond to TUNEL-positive cells.

Figure 5 BID acts downstream of PARP-1 and calpains but upstream of BAX activation, mitochondrial damage, tAIF release, and DNA degradation in MNNG-induced PCD. (**a**) WT and *BID*$^{-/-}$ MEFs were untreated (Control) or treated with MNNG (15 min), immuno-stained for PAR detection (green), and visualized by fluorescent microscopy. Hoechst 33342 (blue) was used to visualize the nuclei. Representative micrographs of each cell type are shown. Bar: 10 μm. After MNNG treatment, the entire WT and *BID*$^{-/-}$ cell population (100% of cells) display PAR-positive labeling. This experiment was repeated six times, yielding similar results display (the entire WT and *BID*$^{-/-}$ cell population display PAR-positive labeling). (**b**) Poly(ADP-ribose) (PAR) immunoblotting detection in lysates from WT and *BID*$^{-/-}$ MEFs untreated or treated with MNNG at different times. The membrane was stained with naphtol blue (NB) to assess protein loading. (**c**) WT and *BID*$^{-/-}$ MEFs were treated with MNNG at the times indicated, and analyzed by measuring absorbance at 570 nm to assess total NAD^+ levels. Concentrations of NAD^+ were normalized to those from untreated cells. Results are the mean of five experiments ± SEM. A pharmacological PARP inhibitor, PJ34, helped to determine the specificity of the PARP-dependent NAD^+ loss associated with MNNG treatment. (**d**) Quantification of the intracellular ATP levels in WT and *BID*$^{-/-}$ MEFs treated with MNNG at different times. H_2O_2 was used as a positive control. 100 % refers to the basal level of ATP scored in untreated cells. Data are the mean of five independent experiments ± SEM. (**e**) Fluorescent assessment of calpain activity measured in WT and *BID*$^{-/-}$ MEFs untreated (Control) or treated with MNNG (1 h). Phase-contrast was used to visualize cells. Representative micrographs of each treatment are shown. After MNNG treatment both WT

and *BID*$^{-/-}$ MEFs (100 %) display calpain-positive staining. This experiment was repeated four times, yielding similar results. Bar: 10 μm. (**f**) WT and *BID*$^{-/-}$ MEFs were treated with MNNG for the indicated times, then labeled with TMRE and assessed for $\Delta\Psi$m by flow cytometry. Results refer to cells with $\Delta\Psi$m loss and are the mean of six independent experiments ± SEM. (**g**) Cytosolic fractions recovered from WT and *BID*$^{-/-}$ MEFs after MNNG treatment at different times were probed for tAIF detection. Actin was used to assess protein loading. (**h**) WT and *BID*$^{-/-}$ MEFs were untreated or treated with MNNG (9 h), stained for the detection of 3'-OH DNA breaks, and analyzed by flow cytometry. Percentages refer to TUNEL-positive cells. This experiment was repeated ten times, with low experimental variability.

Figure 6 BID is cleaved into tBID *via* calpains and localizes in mitochondria during MNNG-induced necroptosis. (**a**) Lysates from MEFs treated by MNNG at the indicated times were prepared and blotted for BID and tBID detection. STS-treated cells were used as a positive control. Alternatively, mitochondrial and cytosolic extracts of cells treated or not with MNNG at different times were analyzed by western blotting for the presence of tBID. STS-treated cells were used as a positive control. Cox IV (mitochondrial marker) and pan-ERK (cytosolic marker) were used to control fractionation quality and protein loading. This experiment was repeated three times, yielding comparable results. (**b**) BID and tBID immunoblotting detection in lysates from WT and *CAPN4*$^{-/-}$ MEFs untreated (Co) or treated with MNNG (9 h) or STS. The membrane was reblotted for actin detection to control protein loading. Note the absence of tBID in MNNG-treated *CAPN4*$^{-/-}$ MEFs. (**c**) WT and *CAPN4*$^{-/-}$ MEFs were treated with MNNG (9 h) or STS, and BAX activation was measured by flow cytometry and illustrated as a bar chart. Data are the means of four independent experiments ± SD. *, $p<0.05$. (**d**) WT and *CAPN4*$^{-/-}$ MEFs were treated or not with MNNG (9 h) or STS, then labeled with TMRE and assessed for $\Delta\Psi$m by flow cytometry. Results refer to cells with $\Delta\Psi$m loss ± SD (n=6). *, $p<0.05$. (**e**) WT and *CAPN4*$^{-/-}$ cells were untreated (Control) or treated with MNNG (9 h) or STS, labeled with AnnexinV and PI, and analyzed by flow cytometry. Representative cytofluorometric plots are shown. Percentages in MNNG-treated cells refer to double positive staining and in STS-treated cells to AnnexinV and PI positive labeling. The red square highlights the absence of cell viability loss recorded in *CAPN4*$^{-/-}$ MEFs after MNNG treatment.

Figure 7 Calpains cleave BID into tBID at Gly70 in MNNG-induced necroptosis. (**a**) Ribbon structure of BID and tBID. Caspases and calpains cleave BID at the D59 and G70

amino acidic position respectively to generate the truncated form of BID (tBID). This processing, which provokes the removal of a part of the BID N-terminus (*red*), discloses the BH3 α helix (*magenta*) on tBID. Here, we represent the tBID generated by calpain processing at G70. (**b**) WT, *BID*$^{-/-}$, *BID*$^{-/-}$ transduced with the pLVX-IRES-Zs-Green lentiviral empty vector (pLV), and two selected clones of *BID*$^{-/-}$ MEFs cells expressing: (i) BID-wt, (ii) a caspase ncBID-D59A mutant, or (iii) two calpain non cleavable (nc)BID mutants (BID-G70A and BID-Δ68-71) were untreated (Control) or treated with MNNG (9 h) and labeled with AnnexinV and PI. The frequency of double positive labeling was recorded and expressed as a plot. Data are the mean ± SD (n=4). The expression level of BID in these cells was assessed by immunoblotting with the help of a V5 monoclonal antibody. Actin was used to control protein loading. (**c**) MEFs were untreated (Control) or MNNG-treated (9 h), and BAX activation was measured by flow cytometry and illustrated as a graph. Data are the means of four independent experiments ± SD. In representative cytofluorometric plots, percentages correspond to cells with active BAX. (**d**) The panel of MEFs used in **b** was untreated (Control) or MNNG-treated (9 h), labeled with TMRE and assessed for ΔΨm by flow cytometry. The frequency of cells with ΔΨm loss was recorded and expressed as a bar chart. Data are the mean of four independent experiments ± SD. (**e**) MEFs left untreated or treated with MNNG (9 h) were subjected to immunoblot detection of BID with the help of a V5 monoclonal antibody. BID-wt and the caspase ncBID-D59A are processed after MNNG treatment (~80 % of BID is cleaved after MNNG treatment, see Materials and Methods section for quantification details). In contrast, the calpain ncBID mutants BID-G70A and BID-D68-71 remain as precursor proteins. Similar results were observed in two independent clones. Actin was used to control protein loading.

Figure 8 Representation of AIF-mediated necroptosis. MNNG-induced DNA damage leads through PARP-1 to NAD^+, ATP depletion and calpain activation. Calpains cleave BID into tBID at Gly70. Once processed, tBID localizes in mitochondria, where it facilitates BAX activation. Furthermore, activated BAX provokes mitochondrial damage and favors the release of tAIF from mitochondria to the cytosol and nucleus. The anti-apoptotic protein BCL-2 can prevent this release. Upon transfer to the nucleus, tAIF associates with CypA and γH2AX to generate a DNA degrading complex that promotes chromatinolysis and cell viability loss.

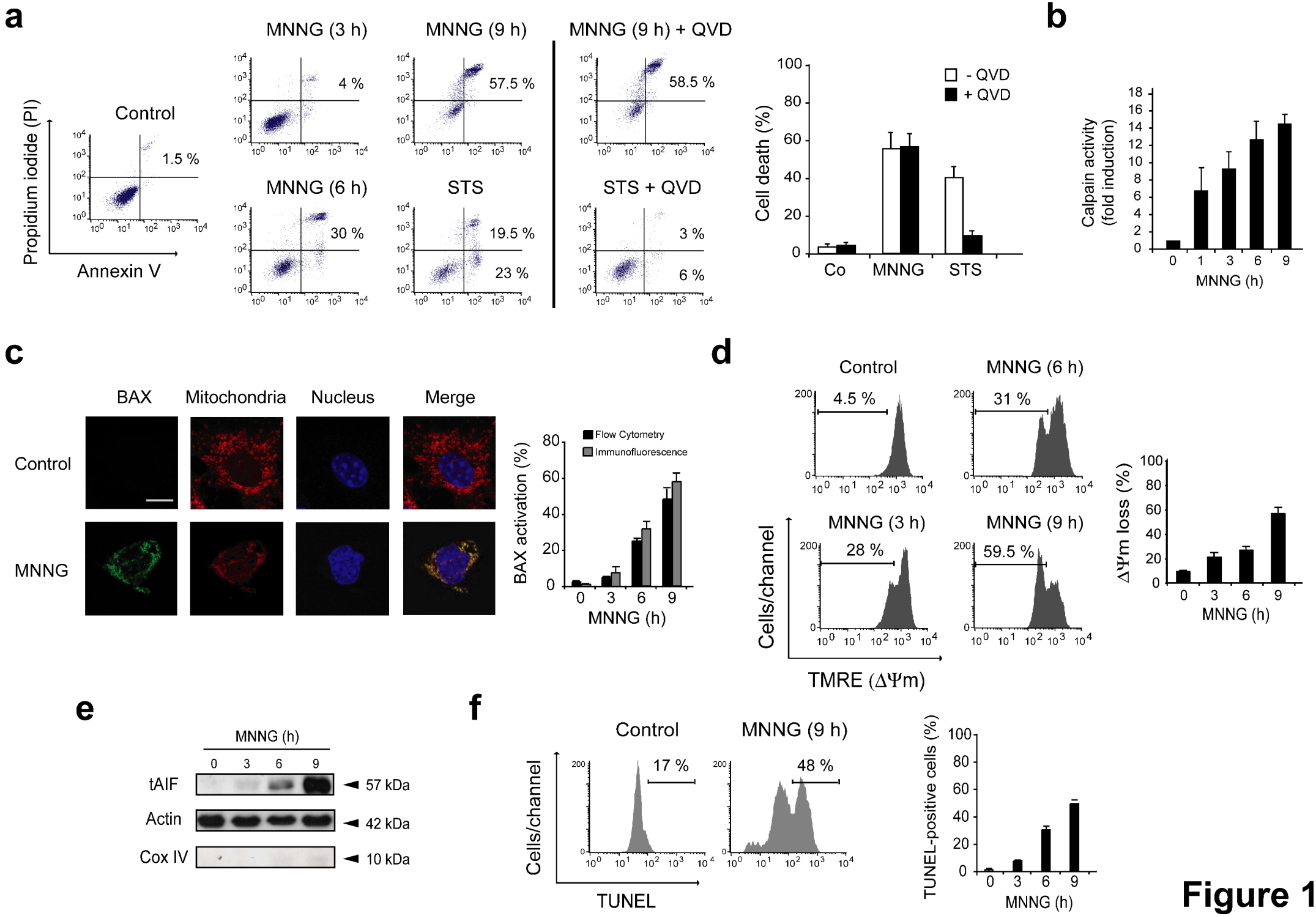
a
MNNG (3 h)
MNNG (9 h)
MNNG (9 h) + QVD
Control
1.5 %
4 %
57.5 %
58.5 %
MNNG (6 h)
STS
STS + QVD
30 %
19.5 %
23 %
3 %
6 %
Propidium iodide (PI)
Annexin V
Cell death (%)
- QVD
+ QVD
Co
MNNG
STS
b
Calpain activity (fold induction)
MNNG (h)
c
BAX
Mitochondria
Nucleus
Merge
Control
MNNG
BAX activation (%)
Flow Cytometry
Immunofluorescence
MNNG (h)
d
Control
MNNG (6 h)
4.5 %
31 %
MNNG (3 h)
MNNG (9 h)
28 %
59.5 %
Cells/channel
TMRE (ΔΨm)
ΔΨm loss (%)
MNNG (h)
e
MNNG (h)
0 3 6 9
tAIF
Actin
Cox IV
57 kDa
42 kDa
10 kDa
f
Control
MNNG (9 h)
17 %
48 %
Cells/channel
TUNEL
TUNEL-positive cells (%)
MNNG (h)

Figure 1

a

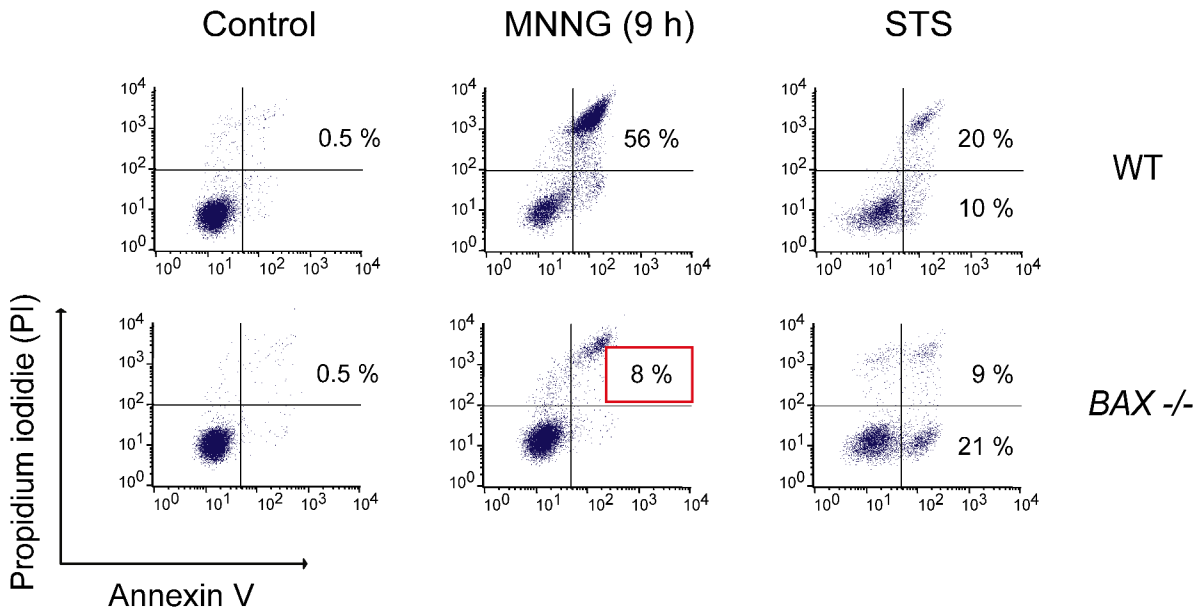
Control
MNNG (9 h)
STS
0.5 %
56 %
20 %
10 %
WT
0.5 %
8 %
9 %
21 %
BAX -/-
Propidium iodidie (PI)
Annexin V

b

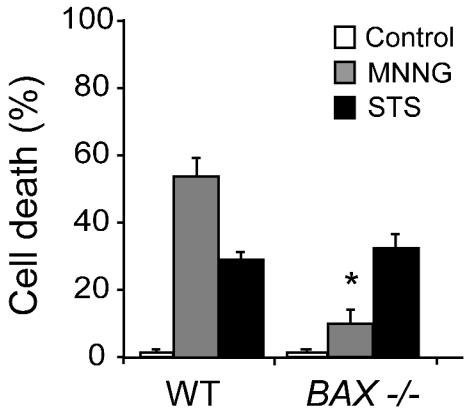
Control
MNNG
STS
Cell death (%)
100
80
60
40
20
0
*
WT
BAX -/-

c

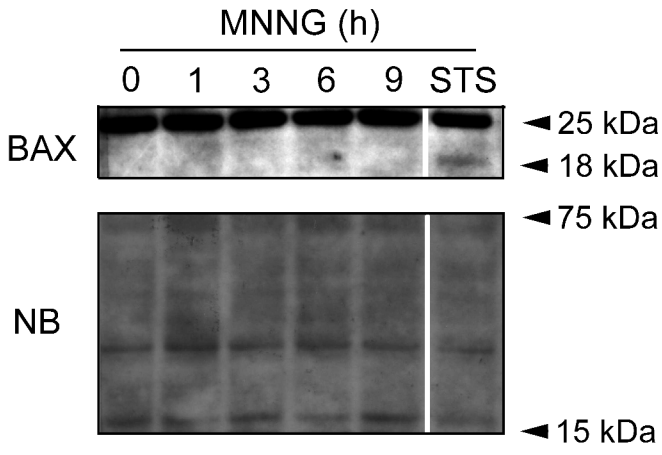
MNNG (h)
0
1
3
6
9
STS
BAX
25 kDa
18 kDa
NB
75 kDa
15 kDa

Figure 2

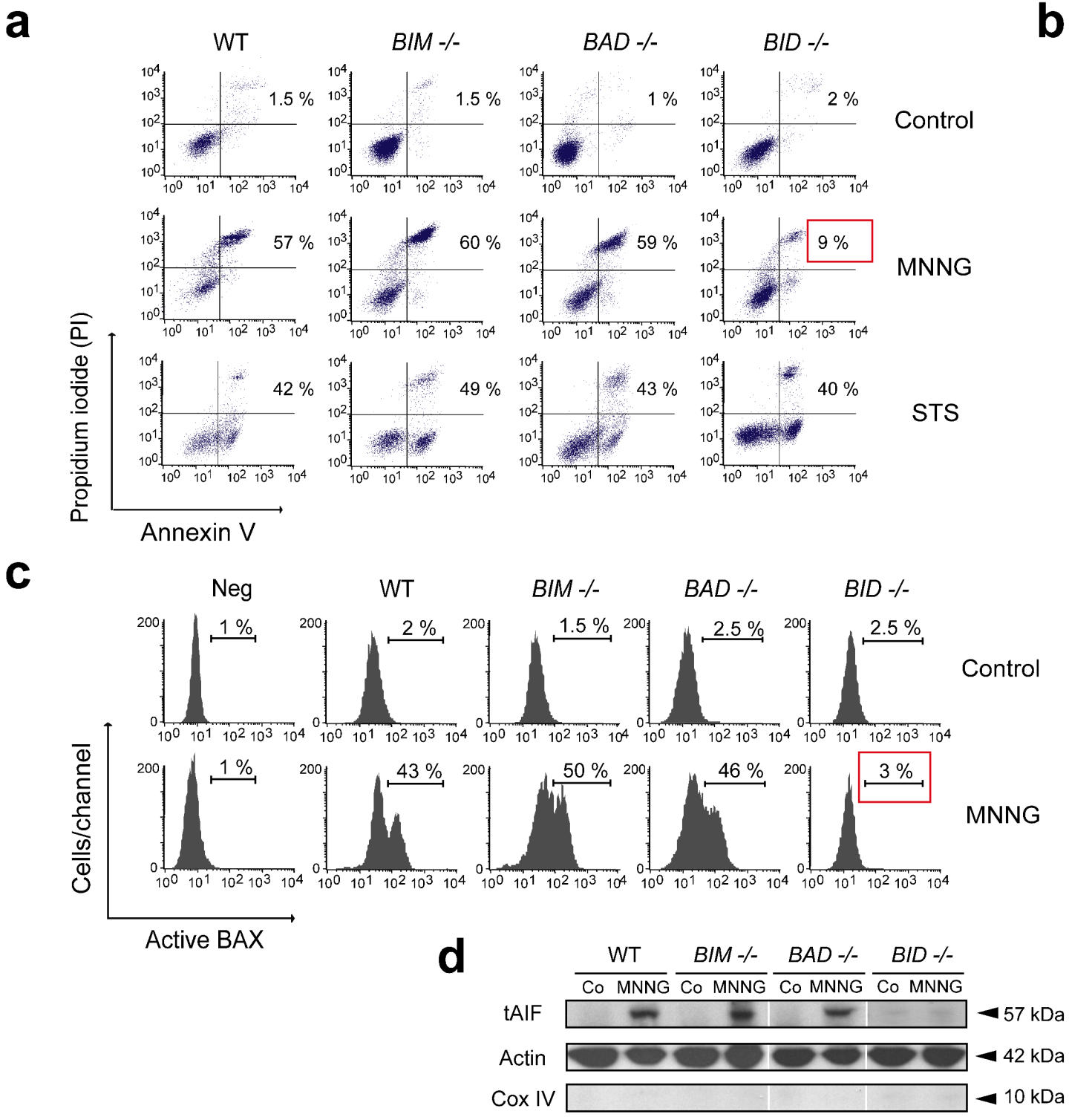
a
WT
BIM -/-
BAD -/-
BID -/-
1.5 %
1.5 %
1 %
2 %
Control
57 %
60 %
59 %
9 %
MNNG
42 %
49 %
43 %
40 %
STS
Propidium iodide (PI)
Annexin V
b
Control
MNNG
Cell death (%)
100
80
60
40
20
0
*
WT
BIM -/-
BAD -/-
BID -/-
c
Neg
WT
BIM -/-
BAD -/-
BID -/-
1 %
2 %
1.5 %
2.5 %
2.5 %
Control
1 %
43 %
50 %
46 %
3 %
MNNG
Cells/channel
Active BAX
BAX activation (%)
d
WT
BIM -/-
BAD -/-
BID -/-
Co
MNNG
tAIF
Actin
Cox IV
57 kDa
42 kDa
10 kDa

Figure 3

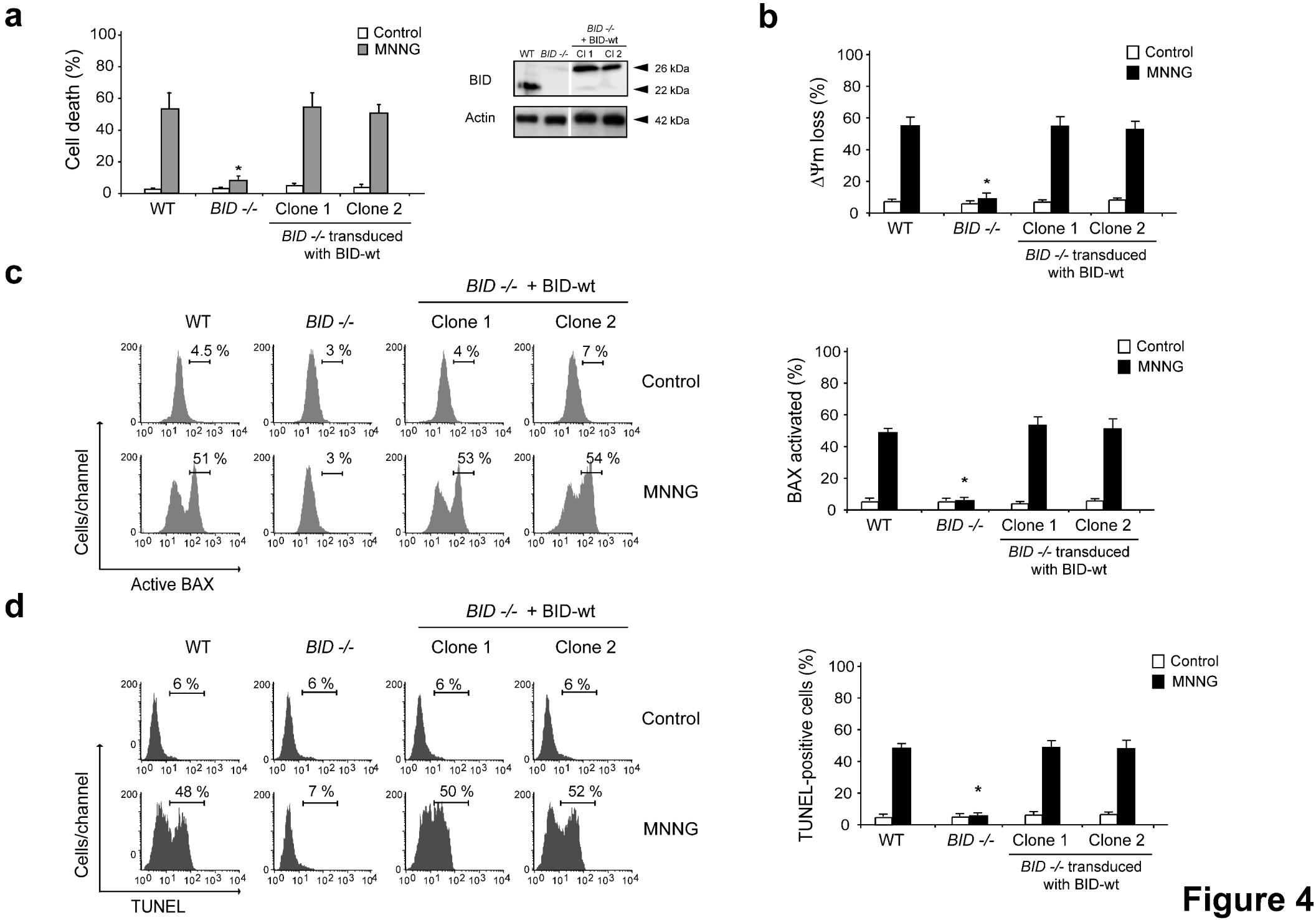
a
Cell death (%)
Control
MNNG
WT
BID -/-
Clone 1
Clone 2
BID -/- transduced with BID-wt
BID -/- + BID-wt
WT BID -/- Cl 1 Cl 2
BID
Actin
26 kDa
22 kDa
42 kDa
b
ΔΨm loss (%)
BAX activated (%)
TUNEL-positive cells (%)
c
BID -/- + BID-wt
Control
MNNG
4.5 %
3 %
4 %
7 %
51 %
53 %
54 %
Cells/channel
Active BAX
d
6 %
48 %
7 %
50 %
52 %
TUNEL

Figure 4

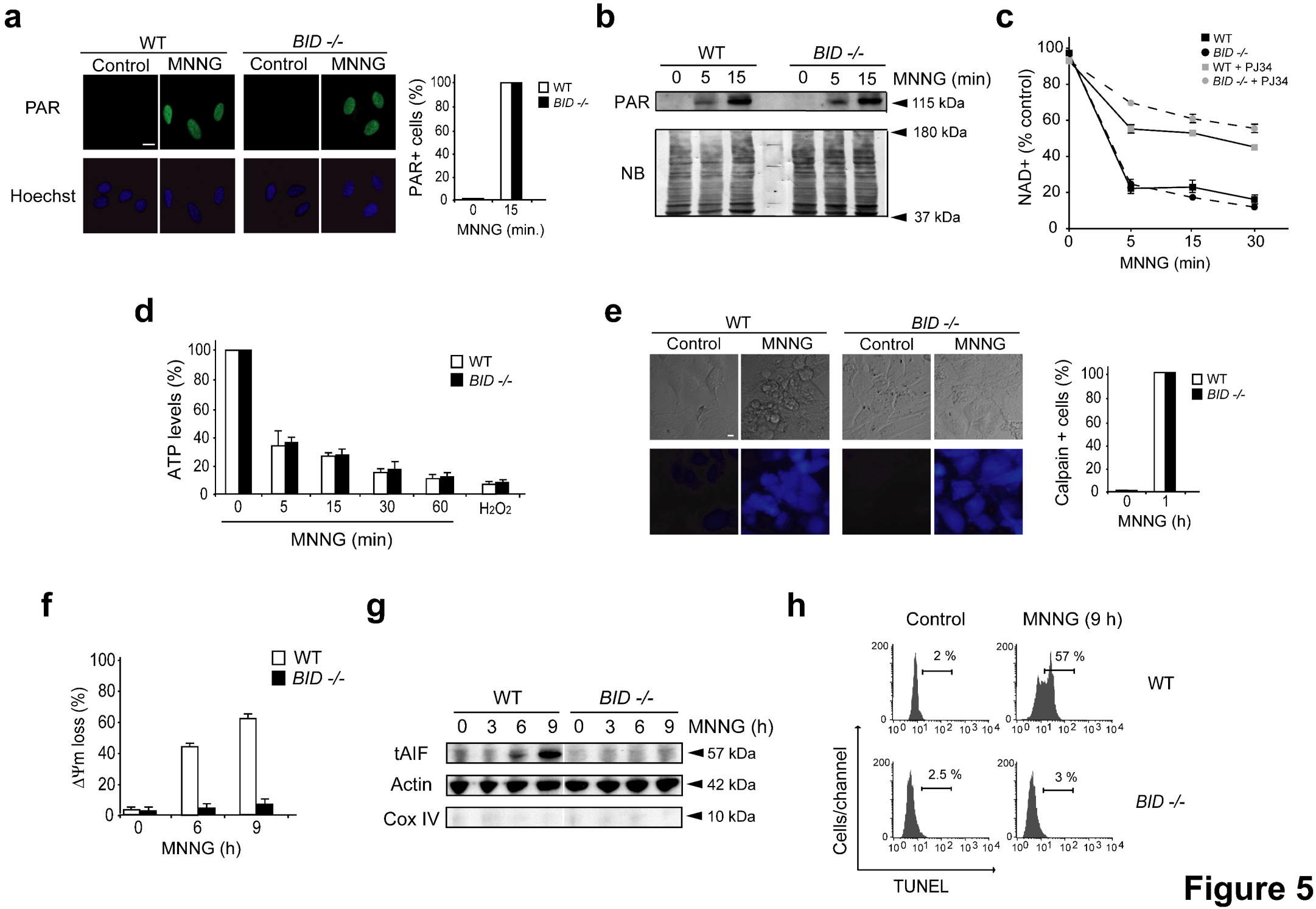
a
WT
BID -/-
Control
MNNG
Control
MNNG
PAR
Hoechst
PAR+ cells (%)
100
80
60
40
20
0
0
15
MNNG (min.)
WT
BID -/-
b
WT
BID -/-
0
5
15
0
5
15
MNNG (min)
PAR
NB
115 kDa
180 kDa
37 kDa
c
WT
BID -/-
WT + PJ34
BID -/- + PJ34
NAD+ (% control)
100
80
60
40
20
0
0
5
15
30
MNNG (min)
d
ATP levels (%)
100
80
60
40
20
0
WT
BID -/-
0
5
15
30
60
H2O2
MNNG (min)
e
WT
BID -/-
Control
MNNG
Control
MNNG
Calpain + cells (%)
100
80
60
40
20
0
WT
BID -/-
0
1
MNNG (h)
f
ΔΨm loss (%)
100
80
60
40
20
0
WT
BID -/-
0
6
9
MNNG (h)
g
WT
BID -/-
0
3
6
9
0
3
6
9
MNNG (h)
tAIF
Actin
Cox IV
57 kDa
42 kDa
10 kDa
h
Control
MNNG (9 h)
2 %
57 %
2.5 %
3 %
WT
BID -/-
Cells/channel
TUNEL

Figure 5

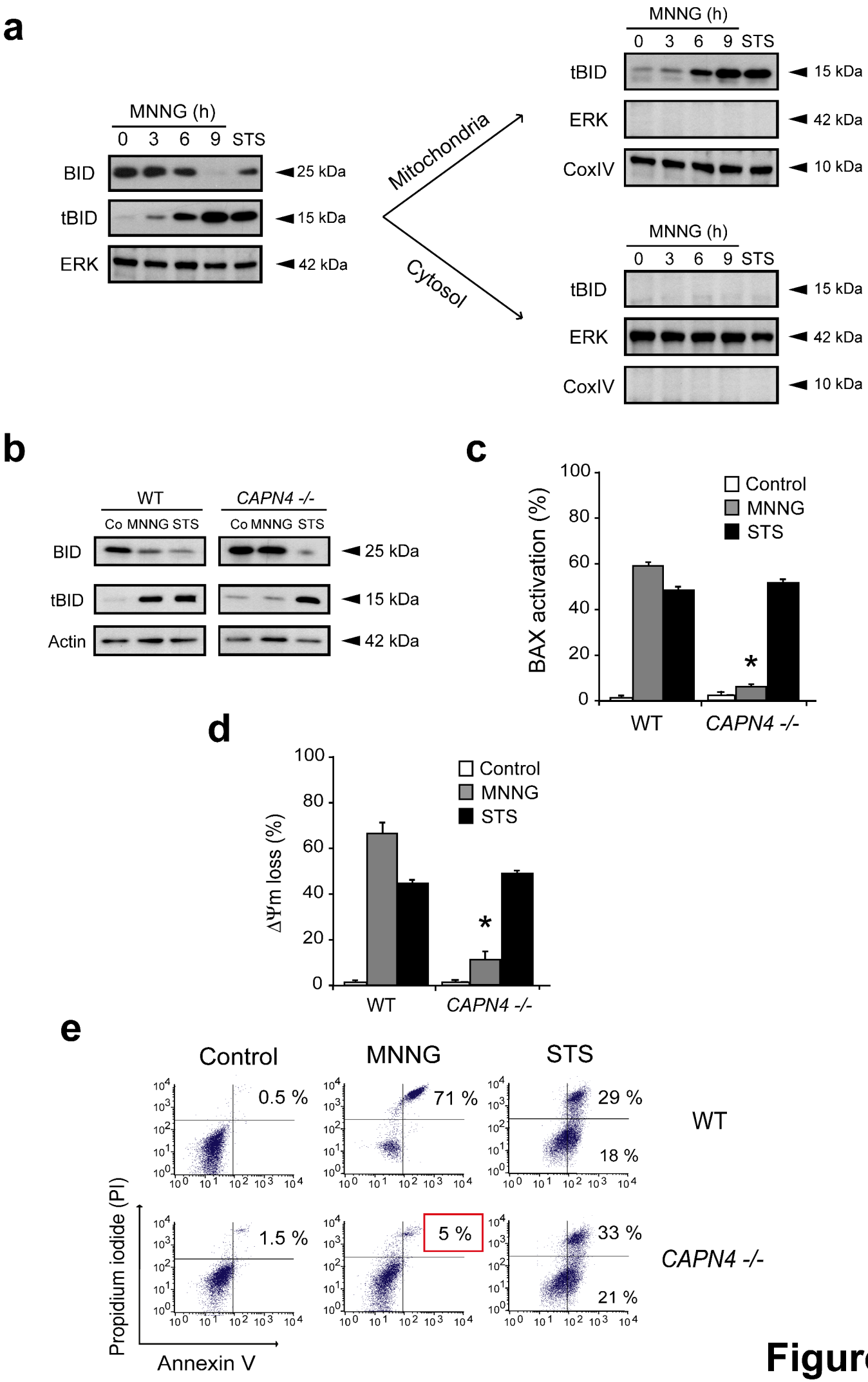
a
MNNG (h)
0 3 6 9 STS
BID
tBID
ERK
25 kDa
15 kDa
42 kDa
Mitochondria
Cytosol
MNNG (h)
0 3 6 9 STS
tBID
ERK
CoxIV
15 kDa
42 kDa
10 kDa
MNNG (h)
0 3 6 9 STS
tBID
ERK
CoxIV
15 kDa
42 kDa
10 kDa
b
WT
CAPN4 -/-
Co MNNG STS
Co MNNG STS
BID
tBID
Actin
25 kDa
15 kDa
42 kDa
c
BAX activation (%)
100
80
60
40
20
0
Control
MNNG
STS
*
WT
CAPN4 -/-
d
ΔΨm loss (%)
100
80
60
40
20
0
Control
MNNG
STS
*
WT
CAPN4 -/-
e
Control
MNNG
STS
0.5 %
71 %
29 %
18 %
1.5 %
5 %
33 %
21 %
WT
CAPN4 -/-
Propidium iodide (PI)
Annexin V

Figure 6

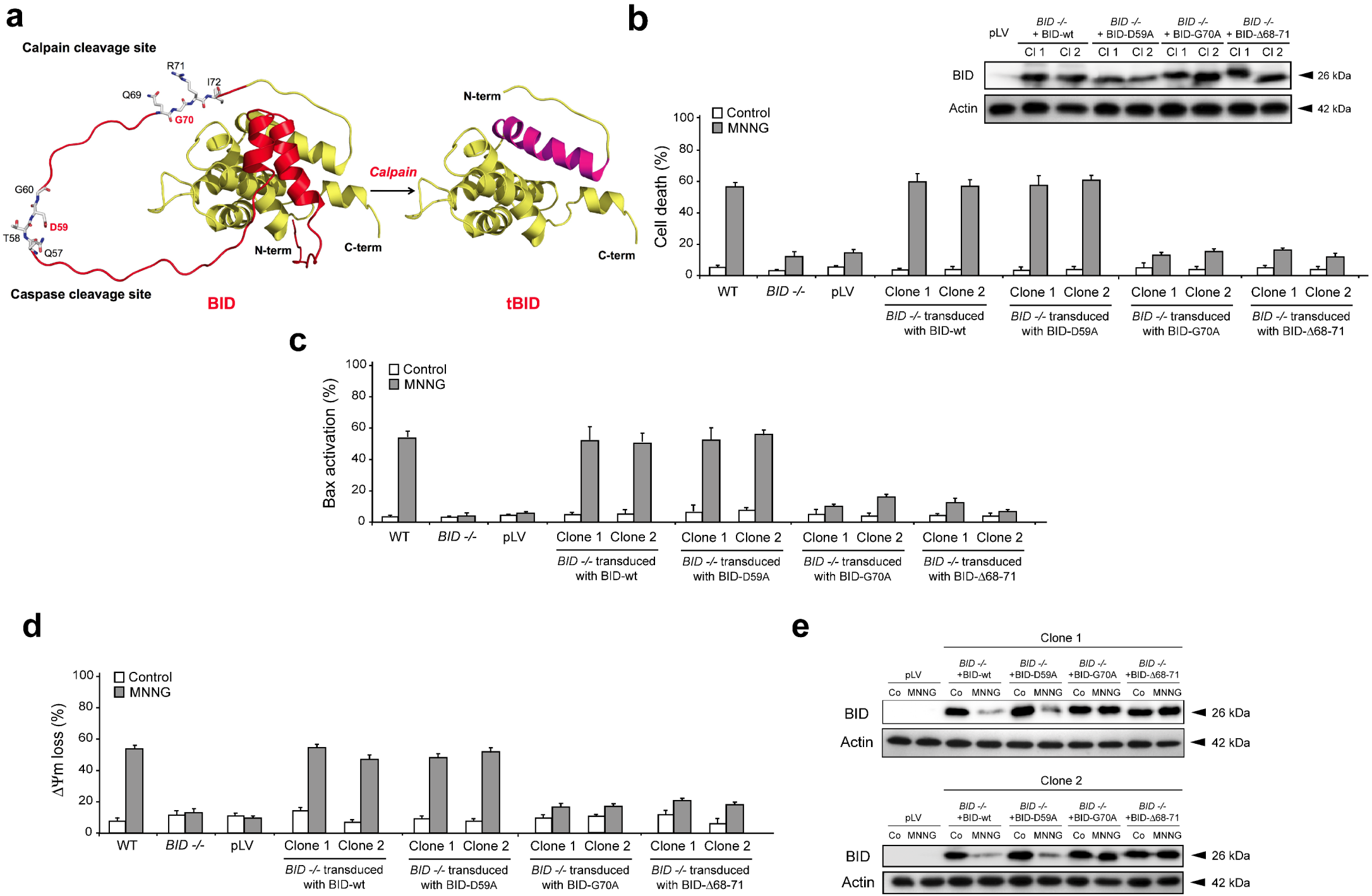
a
Calpain cleavage site
R71
I72
Q69
G70
G60
D59
T58
Q57
N-term
C-term
Calpain
N-term
C-term
Caspase cleavage site
BID
tBID
b
pLV
BID -/- + BID-wt
BID -/- + BID-D59A
BID -/- + BID-G70A
BID -/- + BID-Δ68-71
Cl 1
Cl 2
BID
Actin
26 kDa
42 kDa
Control
MNNG
Cell death (%)
WT
BID -/-
pLV
Clone 1
Clone 2
BID -/- transduced with BID-wt
BID -/- transduced with BID-D59A
BID -/- transduced with BID-G70A
BID -/- transduced with BID-Δ68-71
c
Bax activation (%)
d
ΔΨm loss (%)
e
Clone 1
Clone 2
Co
MNNG

Figure 7

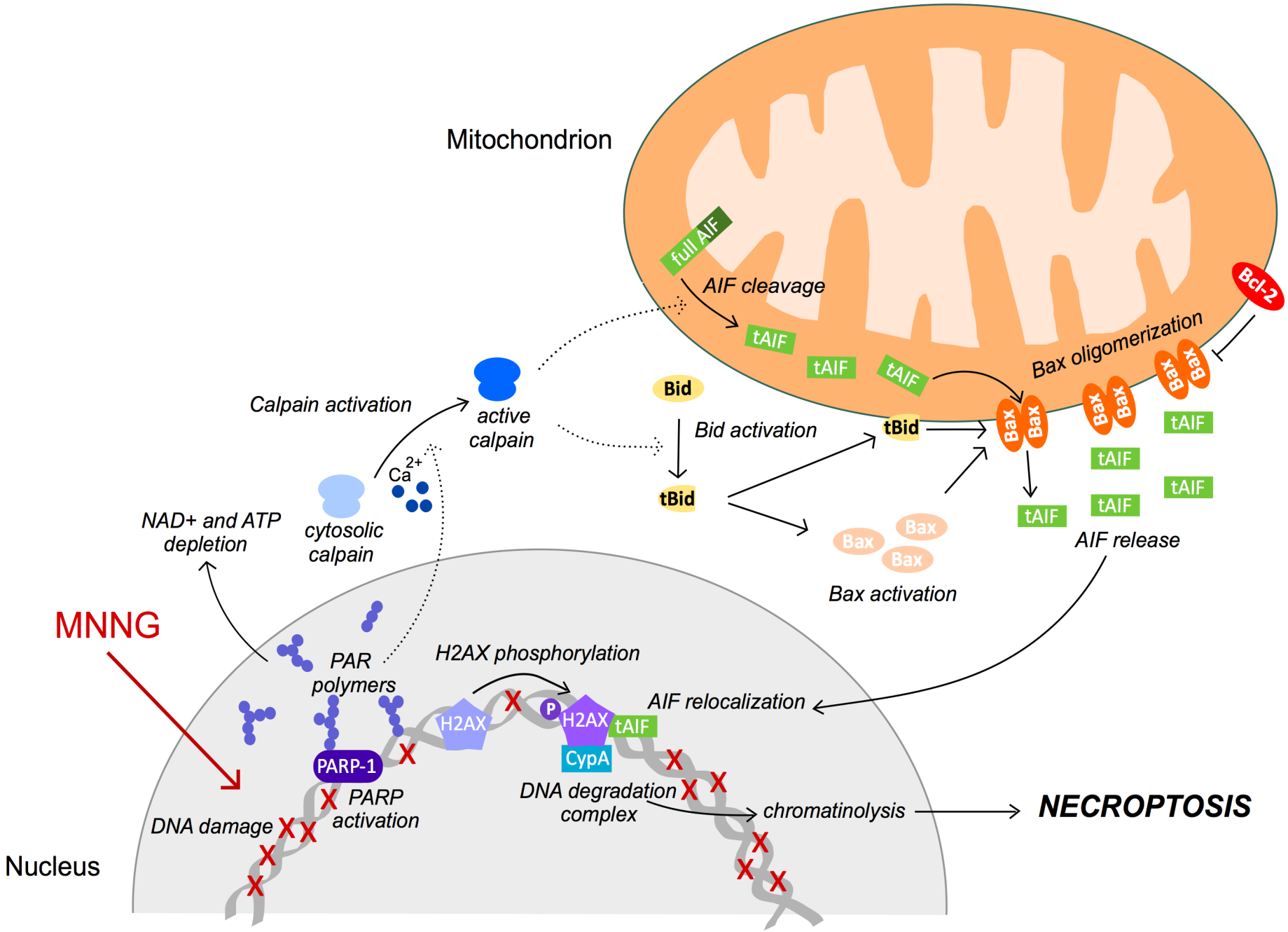
Mitochondrion
full AIF
AIF cleavage
tAIF
tAIF
tAIF
Bcl-2
Bax oligomerization
Bax
Bax
Bax
Bax
tAIF
tAIF
tAIF
tAIF
tAIF
AIF release
Calpain activation
active calpain
Ca2+
cytosolic calpain
Bid
Bid activation
tBid
tBid
Bax
Bax
Bax activation
NAD+ and ATP depletion
MNNG
PAR polymers
H2AX phosphorylation
H2AX
P
H2AX
tAIF
CypA
AIF relocalization
PARP-1
PARP activation
DNA damage
DNA degradation complex
chromatinolysis
NECROPTOSIS
Nucleus

Figure 8